Amplified and tunable transverse and longitudinal spin-photon coupling in hybrid circuit-QED

Neill Lambert,[1] Mauro Cirio,[1] Matthieu Delbecq,[1] Giles Allison,[1] Marian Marx,[1,2] Seigo Tarucha,[1,2] and Franco Nori[1,3]

[1]*CEMS, RIKEN, Saitama 351-0198, Japan*

[2]*Department of Applied Physics, University of Tokyo, Bunkyo-ku, Tokyo 113-8656, Japan*

[3]*Department of Physics, University of Michigan, Ann Arbor, Michigan 48109-1040, USA*

We describe a method to tune, *in situ*, between transverse and longitudinal light-matter coupling in a hybrid circuit-QED device composed of an electron-spin degree of freedom coupled to a microwave transmission line cavity. Our approach relies on periodic modulation of the coupling itself, such that in a certain frame the interaction is both amplified and either transverse or, by modulating at two frequencies, longitudinal. The former realizes an effective simulation of certain aspects of the ultra-strong-coupling regime, while the latter allows one to implement a longitudinal readout scheme even when the intrinsic Hamiltonian is transverse, and the individual spin or cavity frequencies cannot be changed. We analyze the fidelity of using such a scheme to measure the state of the electron-spin degree of freedom, and argue that the longitudinal readout scheme can operate in regimes where the traditional dispersive approach fails.

I. INTRODUCTION

Electron spin is a highly robust quantum degree of freedom the use of which in quantum information is often limited by the difficulty of implementing fast high-fidelity readout and the realization of long-distance interactions [1–5]. Spin-photon coupling in hybrid devices composed of double quantum dots (DQDs) coupled to superconducting transmission line cavities is being investigated and developed as a means to overcome these difficulties [5–19]. Very recently several experiments have demonstrated strong spin-photon coupling [20–22] based on coupling mediated by the charge degree of freedom [23,24–26]. In addition to applications in quantum information, such devices harbor new physics, including controllable single-atom lasing [27–30], ground-state lasing [31], bistability [32], nonequilibrium thermodynamics [33], and quantum phase transitions [34].

In this paper we focus on the practical task of how to switch [19], *in situ*, between an amplified *longitudinal* [35–40] and an amplified *transverse* coupling, by only modulating the coupling strength, and without changing the spin or cavity energies directly. With the former (amplified longitudinal coupling) one can realize fast high-fidelity readout [35] and qubit-qubit coupling [36]. With the latter (amplified transverse coupling) one can investigate the extreme limits of light-matter coupling [41–47] in a simulated manner [48–52].

Our primary result is that one can realize an effective amplified longitudinal coupling even when there is a non-negligible intrinsic transverse term in the Hamiltonian by modulating the coupling strength at *both the cavity and qubit frequencies simultaneously* (two-tone), and moving to an appropriate frame. We show that this works optimally when the intrinsic qubit frequency is half of the cavity frequency. The effect can be intuitively understood in terms of a simultaneous resonant force on the cavity and electron-spin resonance on the qubit. We say that the coupling strength is amplified in the

sense that the influence of the qubit on the cavity is increased drastically as the effective cavity frequency is reduced.

With the electron-spin-based devices we discuss in this paper this modulation is potentially achievable with electrical control of a single gate voltage [36,53]. This method is particularly desirable when, as is the case we outline below, one cannot (or may not want to) directly engineer a longitudinal interaction, or cannot control *in situ* the intrinsic properties of the device (other than the coupling itself). The two-tone approach [54], similar in philosophy to stroboscopic schemes [55,56], also has the advantage that, when used as a means to measure the qubit state, it is faster than dispersive readout, and can still operate well in the limit of strong coupling and a bad cavity [56]. The downside is that, like the normal dispersive readout scheme, it is approximate, and the quantum nondemolition (QND) nature of the measurement breaks down away from ideal parameters (unlike an ideal intrinsic longitudinal coupling). Thus the longitudinal readout part of our paper lies between the "pure" longitudinal case and the traditional dispersive case, with the fast readout of the former, and the potentially easier implementation of the latter (albeit with corresponding limits to its intrinsic QND fidelity away from an optimal choice of parameters).

First we describe the basic elements of the spin-photon coupling mechanism. We then introduce the modulated coupling, and discuss how the two-tone modulation allows us to realize a longitudinal coupling even when the intrinsic Hamiltonian is transverse. We then analyze the fidelity of a two-tone longitudinal measurement scheme, and show how it compares to the normal longitudinal readout (with only a single-tone modulation of the coupling) and dispersive readout approaches. We investigate the influence of unwanted exchange tunneling terms, and then finally discuss how a single-tone modulation can give an amplified transverse coupling. In the Appendix, we present a detailed analysis of the perturbative limits of the two-tone modulation approach.

II. ORIGIN OF THE SPIN-PHOTON COUPLING

Following the approach of Ref. [53] we consider a model of a DQD operating in the two-electron regime, and at the charge-degeneracy point to minimize dephasing. A microwave resonator modifies the gate voltage that controls the interdot tunneling, which results in a spin-photon coupling as described below. In addition, the electrons in the dots are subject to an external magnetic field $B_{\mathrm{ex}} = B\hat{z}$, separating the triplet states, $T_+ = |\uparrow\uparrow\rangle$ and $T_- = |\downarrow\downarrow\rangle$, from the triplet state, $T_0 = (|\uparrow\downarrow\rangle + |\downarrow\uparrow\rangle)/\sqrt{2}$, and the singlet state, $S = (|\uparrow\downarrow\rangle - |\downarrow\uparrow\rangle)/\sqrt{2}$. For brevity we neglect reference to the corresponding spatial orbital wave functions [57–60] of the electrons in the double dot. The electrons are also subject to inhomogeneous magnetic fields B_L and B_R, originating from either inhomogeneous nuclear Overhauser fields or the strong gradient field of a micromagnet. Here, we define

$$\sigma_z = |\downarrow\uparrow\rangle\langle\downarrow\uparrow| - |\uparrow\downarrow\rangle\langle\uparrow\downarrow| \equiv |T_0\rangle\langle S| + |S\rangle\langle T_0|, \quad (1)$$

$$\sigma_x = |\downarrow\uparrow\rangle\langle\uparrow\downarrow| + |\uparrow\downarrow\rangle\langle\downarrow\uparrow| \equiv |T_0\rangle\langle T_0| - |S\rangle\langle S|. \quad (2)$$

Within this restricted two-state subspace the Hamiltonian for the spin states of the dots is given by

$$H_d = \frac{J_0}{2}\sigma_x + \frac{\Delta h}{2}\sigma_z, \quad (3)$$

where J_0 is the exchange tunneling [57,59,60] and $\Delta h = g_e \mu_B (B_L - B_R)$ is the difference in local Zeeman energies. In this paper we focus on the regime where $\Delta h \gg J_0$.

We assume that the superconducting transmission line is coupled to the interdot tunnel gate. The vacuum state in the cavity has a nonzero voltage that can modify this barrier, and thus induces a Hamiltonian,

$$H_c = \omega_c a^\dagger a + J_r \sigma_x (a + a^\dagger), \quad (4)$$

where ω_c is the resonant cavity frequency and J_r is the spin-photon coupling strength (see below). Reference [53] considers the eigenstates of H_d as the qubit basis, and by applying a large *global* magnetic field the authors propose tuning $J_0 \to 0$, to maximize the *transverse* spin-boson coupling. One downside to this approach, however, is that this mechanism of tuning J_0 to zero is, to our knowledge, as yet unobserved in experiments. It also requires strong external magnetic fields, which, depending on design, may be incompatible with the critical field requirements of a superconducting transmission line resonator, and may also reduce the intrinsic strength of J_r. In addition, Ref. [53] suggests that the opposite longitudinal regime can be reached by tuning the Zeeman splitting Δh, such that it is much smaller than the exchange tunneling J_0.

Here, we investigate a complementary approach to this notion of switching between longitudinal and transverse interactions, based purely on modulation of the coupling strength between the cavity and double quantum dot. As mentioned in the Introduction, this also allows us to realize fast longitudinal-coupling readout [35]. This on-chip tunability is particularly beneficial to certain double quantum dot devices where it may be difficult to tune Δh *in situ*, and where an inherently large Δh may be desirable for state-preparation purposes.

A. Driven coupling

In Ref. [53] the functional dependence of the exchange-tunneling mediated spin-photon coupling J_r is given by

$$J_r(t) = eV_r \sinh\left[\frac{16V_h(t)\left(\omega_0^2 + 2\omega_L^2\right)}{\hbar\omega_0^2\sqrt{\omega_0^2 + \omega_L^2}}\right]^{-1} \quad (5)$$

where $\omega_L = eB/2m$ is the Larmor frequency, ω_0 is the frequency of the harmonic well defining each dot, and V_h is the height of the tunnel barrier between the two dots. Essentially, the vacuum-fluctuation induced voltage V_r modifies the height of the tunnel barrier, which in turn changes the exchange splitting between triplet and singlet states [57,59,60]. The height V_h is in practice a tunable parameter which can be controlled by a gate voltage. By applying time-dependent driving [61] to this gate voltage, $V_h(t)$, one can make $J_r(t)$ time dependent. One caveat is, in the same stroke, we also induce a time dependence in the exchange tunneling, J_0, itself. However, as discussed in the different context of superconducting qubits [35], this type of imperfection typically has a minimal influence of the fidelity or QND-ness of the measurement (as we will discuss below).

Using exchange tunneling to realize modulated coupling is not the only potential way to implement this tunable spin-photon coupling scheme. Following the proposal described in Ref. [8] one could couple the spin of a single electron in a double dot structure to the microwave cavity by applying a strong magnetic field gradient with a micromagnet [20,21]. This could then be made time dependent by electrical control of the dot potential [19,62], or modulation of the field gradient with a suspended nanomagnet [63]. There are various advantages and disadvantages to using single spin versus an effective singlet-triplet qubit. The latter tends to have worse dephasing than the former when the exchange tunneling or the dot bias are changed [8], but has the advantage of being well developed in terms of electrical preparation and readout of the qubit state.

III. TWO-TONE DRIVING AND AMPLIFIED LONGITUDINAL READOUT

When $\Delta h \gg J_0$ our intrinsic Hamiltonian is transverse, and we assume Δh is a static property that cannot be tuned *in situ*. However, as mentioned in the introduction, we can access an effective amplified longitudinal regime by driving the coupling at two frequencies. When the natural splitting of the qubit and cavity are off-resonance ($\Delta h \sim \omega_c/2$), we can do quasi-QND amplified longitudinal readout of the σ_x basis, as we have defined it. More specifically, returning again to the Hamiltonian

$$H = \omega_c a^\dagger a + \frac{\Delta h}{2}\sigma_z + J_r(t)\sigma_x(a + a^\dagger) \quad (6)$$

and choosing

$$J_r(t) = J_r \cos(\omega_c t)\cos(\Delta h t) \quad (7)$$

and moving to a rotating frame under the unitary transformation $U = \exp i[\omega_c a^\dagger a + (\Delta h/2)\sigma_z]t$, under the assumptions that $\omega_c, \Delta h \gg J_r$, and neglecting fast oscillating terms [64] of frequency $2\omega_c, 2\Delta h, \omega_c + \Delta h$, and $\omega_c - \Delta h$ (the neglect of
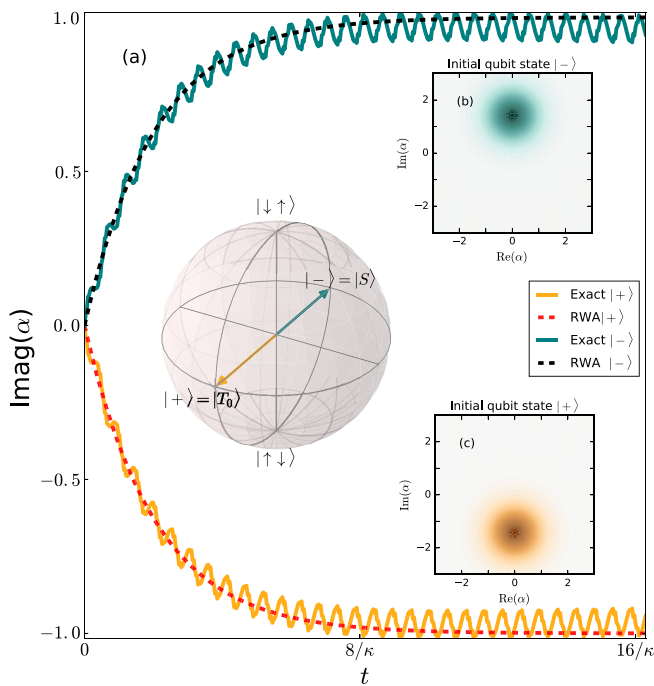
FIG. 1. (a) An example of the evolution of the imaginary part of the cavity state $\alpha = \langle a \rangle$ when the qubit is prepared in the $\langle + \rangle$ or $\langle - \rangle$ eigenstate of the σ_x for the two-tone modulated longitudinal readout scheme. Note that in our notation the scheme is longitudinal in the σ_x basis, and is quasi-QND in that basis, as shown by the Bloch sphere inset. The dashed curves show the approximate RWA solution, while the solid lines show the full numerics, which includes oscillations due to the counter-rotating terms. The insets (b) and (c) show the Wigner function of the cavity state for the different initial qubit states at $t = 16/\kappa$. In this figure we have used nonideal parameters to accentuate the unwanted oscillations, with $\Delta h = 0.15\omega_c$, $J_r = 0.05\omega_c$, and $\kappa = J_r/2$. The oscillations due to counterterms reduce the QND fidelity of the measurement, but this can be improved by of course increasing Δh or reducing the coupling strength J_r [and correspondingly reducing κ to maintain the same signal magnitude $\alpha(t \to \infty) = J_r/2\kappa$.]

which relies on $\omega_c, \Delta h, \omega_c - \Delta h \gg J_r$), we obtain

$$H_0 = \frac{J_r}{4}\sigma_x(a + a^\dagger).$$
(8)

Thus, we have effectively entered a frame where both the cavity frequency (as in the previous section) and the qubit splitting are zero. This Hamiltonian thus describes a σ_x-dependent resonant force on the cavity, and with it we can perform fast quasi-non-QND readout of the eigenstates of that basis (albeit in a rotating frame). It is more traditional to redefine the basis states to measure in σ_z, but we refrain from doing so. With this Hamiltonian the qubit-dependent displacement of the cavity tends towards

$$\alpha = \langle a \rangle = \pm J_r/2i\kappa$$
(9)

in the steady state, as shown in Fig. 1, and does so faster than the equivalent dispersive interaction [35] (here κ is the cavity loss rate; see below for a full description). If one prefers to perform a measurement in the σ_z basis one must of course initially apply a rotation on the qubit before the measurement is performed.

The validity of Eq. (8) depends strongly on

$$\omega_c, \Delta h \gg J_r$$
(10)

and

$$\omega_c - \Delta h \gg J_r.$$
(11)

In a regime where $J_r/8 < \Delta h < \omega_c - J/8$, the leading non-QND terms are, asymptotically,

$$O\{\max[J_r^2/\Delta, J_r^2/(\omega_c - \Delta)]\},$$
(12)

suggesting an optimal point of

$$\omega_c = 2\Delta h$$
(13)

(see the Appendix for details). Explicitly, using Van-Vleck perturbation theory (see the Appendix for the derivation), the lowest-order non-QND terms are

$$H^{\text{VV}} = H_0 + \left(\frac{J_r}{4}\right)^2 \left[\frac{(a + a^\dagger)^2}{2\Delta h}\right.$$
$$\left. - \frac{\Delta h}{\omega_c^2 - \Delta h^2}\left(a^\dagger a + \frac{1}{2}\right)\right]\sigma_z.$$
(14)

We validate this analysis with a numerical simulation of the full dynamics [65,66], which involves solving a master equation including the full time-dependent Hamiltonian Eq. (6) and cavity loss rate κ:

$$\dot{\rho} = -\frac{i}{\hbar}[H(t), \rho] + \frac{\kappa}{2}[2a\rho a^\dagger - a^\dagger a\rho - \rho a^\dagger a].$$
(15)

Here we neglect qubit (DQD) loss and dephasing, and focus only on the influence of the cavity losses by assuming that κ is the largest loss rate in our system. This assumption is complementary to the benefit that the longitudinal readout scheme works well in the bad cavity limit.

Figures of merit for the efficiency of the readout scheme are the nondestructiveness (QND-ness) and the time-dependent signal-to-noise ratio (SNR). In Fig. 2, from the full numerical results, we show a simple measure, $\text{Min}[\langle + | + \rangle]_\tau$, of the nondestructiveness of the measurement in terms of the minimum overlap between the state of the qubit (in the rotating frame) and the initial state $|+\rangle$, across the whole time evolution interval τ, as a function of Δh. Note that, at this stage, we tune across a large range of Δh, but always assume that $\Delta h \gg J_0$, even when $\Delta h \to 0$. This is because we wish to first show the breakdown of our approach due to the failure of the rotating-wave approximation (RWA) leading to Eq. (8). We will address the issue of finite J_0 in the next section.

At $\Delta h = 0$, we retrieve the purely longitudinal results of Didier *et al.* [35]. As Δh increases, readout relying on a single-tone modulation of the coupling just at the cavity frequency of course fails to produce a satisfactory QND-ness, as shown by the gray dashed curve. However, by modulating at two frequencies (solid curve) we observe first a drop in the QND-ness, and then right afterwards we see a revival, as the simplified RWA model Eq. (8), which predicts ideal nondestructive measurement at $\Delta h = \omega_c/2$, becomes valid (see the Appendix).

The time-dependent signal-to-noise ratio is given by

$$\text{SNR}(\tau) = \frac{\langle M(\tau)_+ \rangle - \langle M(\tau)_- \rangle}{[\langle \delta M(\tau)_+^2 \rangle + \langle \delta M(\tau)_-^2 \rangle]^{1/2}},$$
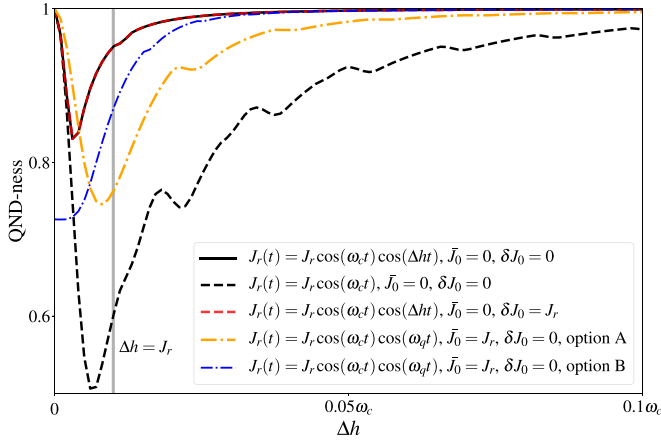(16)

FIG. 2. As a figure of merit of the QND fidelity of the measurement process we use for an initial excited state $|+\rangle$, i.e., $\text{Min}[\langle|+\rangle\langle+|\rangle]_\tau$, and we take the maximum evolution time as $\tau = 2/\kappa$. Here we use parameters closer to those expected in a DQD-cavity setup, with $\omega_c/2\pi = 5$ GHz, $J_r/2\pi = 50$ MHz, and $\kappa/2\pi = 25$ MHz. In the black curve we set the static exchange tunneling to zero, $J_0 = 0$, and we tune $\Delta h/2\pi$ across the range 0–250 MHz (the magnitude of J_r is indicated by the vertical gray line). The black dashed curve shows the same except with a modulation of the spin-photon coupling just at the cavity frequency alone. When $\Delta h = 0$ we recover the pure longitudinal result of Didier *et al.* [35]. As Δh is increased, the QND-ness of the two-tone modulation scheme decreases until a critical turning point, corresponding to the passage from an adiabatic regime to a fast-modulation regime, where the RWA starts to become valid. This regime is ideal when $\Delta h = \omega_c/2$ (see the Appendix for a complete analysis), but we see that, for the parameters in this example, it already performs well as $\Delta h \to \omega_c/20$. The red dashed curve shows the influence of a modulated exchange tunneling, $\delta J_0/2\pi = J_r/2\pi = 50$ MHz. The dashed orange curve shows the influence of a static exchange tunneling, $\bar{J}_0/2\pi = J_r/2\pi = 50$ MHz, following strategy A for preparation and readout, described in the text. The dash-dotted blue curve shows the influence of a static exchange tunneling, $\bar{J}_0/2\pi = J_r/2\pi = 50$ MHz, following strategy B for preparation and readout, also described in the text. In the cases with static exchange coupling present, we modulate the spin-photon coupling at the eigenenergy of the dot system $\omega_q = \sqrt{\Delta h^2 + \bar{J}_0^2}$.

where $+$ and $-$ refer to the qubit state in the σ_x basis, and

$$M(\tau) = \sqrt{\kappa} \int_0^\tau dt \, [a_{\text{out}}^\dagger(t) + a_{\text{out}(t)}] \quad (17)$$

is the homodyne signal in terms of the integrated quadrature amplitude of photons leaking out of the cavity at a rate κ [where $a_{\text{out}}(t) = \sqrt{\kappa} a(t) + a_{\text{in}}(t)$ includes vacuum noise $\langle a_{\text{in}}(t) a_{\text{in}}^\dagger(t') \rangle = \delta(t - t')$]. The integrated noise is given by the sum of the variance of both outcomes, $\delta M(\tau) = M(\tau) - \langle M(\tau) \rangle$, which can be evaluated as [67,68]

$$\delta M(\tau)^2 = \kappa^2 \int_0^\tau dt \int_0^\tau dt' (\text{Tr}[(a + a^\dagger) \exp\{\mathcal{L}(t' - t)\}$$
$$\times (a\rho(t) + \rho(t)a^\dagger)]u(t' - t)$$
$$+ \text{Tr}[(a + a^\dagger) \exp\{\mathcal{L}(t - t')\}(a\rho(t')$$
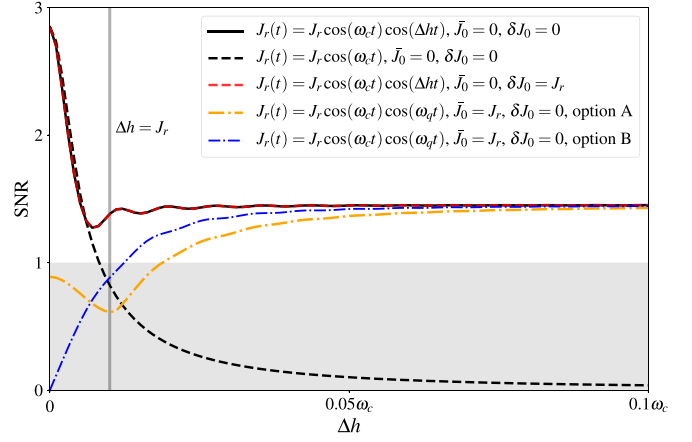$$+ \rho(t')a^\dagger)]u(t - t')) + \kappa\tau - \langle M(\tau) \rangle^2, \quad (18)$$

FIG. 3. Here we show the integrated signal-to-noise ratio obtained up to time $\tau = 2/\kappa$, as a function of Δh, with other parameters set as in Fig. 2, $\omega_c/2\pi = 5$ GHz, $J_r/2\pi = 50$ MHz, and $\kappa/2\pi = 25$ MHz. The black curve shows that SNR is maximal for $\Delta h \to 0$, then drops and saturates as Δh is increased (the magnitude of J_r is indicated by the vertical gray line). The black dashed curve shows the same except with modulation of the spin-photon coupling just at the cavity frequency alone. The red dashed curve shows the influence of a modulated exchange tunneling, $\delta J_0/2\pi = J_r/2\pi = 50$ MHz. The dashed orange curve shows the influence of a static exchange tunneling, $\bar{J}_0/2\pi = J_r/2\pi = 50$ MHz, following strategy A for preparation and readout, described in the text. The dash-dotted blue curve shows the influence of a static exchange tunneling, $\bar{J}_0/2\pi = J_r/2\pi = 50$ MHz, following strategy B for preparation and readout, also described in the text. In the cases with static exchange coupling present, we modulate the spin-photon coupling at the eigenenergy of the dot system $\omega_q = \sqrt{\Delta h^2 + \bar{J}_0^2}$.

which, in the case that the state in the cavity is a coherent state, reduces to $\delta M(\tau)^2 = \kappa\tau$, where τ is the total measurement period. Here, the step functions are defined as $u(t) = 1$ for $t > 0$ and $u(t) = 0$ for $t < 0$.

In Fig. 3 we show the signal-to-noise ratio, Eq. (16), also as a function of Δh, up to a maximum integration time of $\tau = 2/\kappa$. The larger SNR at $\Delta h = 0$ is ultimately due to the effectively larger coupling J_r, compared to the case when one has a finite frequency of modulation (i.e., at $\Delta h = 0$, J_r is effectively two times larger compared to when the modulation at finite Δh occurs, and whence averaging over fast oscillations effectively reduces the coupling strength). As Δh increases, as with Fig. 2, modulating the coupling at just a *single* frequency is accompanied with a loss of signal. However, if one modulates at *two* frequencies, ω_c and Δh, the SNR plateaus, as expected from Eq. (8) and the analysis performed in Ref. [35].

In comparing their pure longitudinal measurement scheme to the traditional dispersive approach, Ref. [35] argued that the SNR of the longitudinal scheme increases faster than that of the dispersive one at short times:

$$\text{SNR}(\tau) \propto \frac{1}{\kappa}(\kappa\tau)^{5/2} \quad \text{for the dispersive case,}$$

$$\text{SNR}(\tau) \propto \frac{1}{\kappa}(\kappa\tau)^{3/2} \quad \text{for longitudinal readout,}$$

$$\text{SNR}(\tau) \propto \frac{1}{\kappa}(\kappa\tau)^{1/2} \quad \text{for both at longer times} \quad \tau \gg \kappa^{-1}.$$

While this is also the case for the two-tone readout, we point out an additional advantage of both the purely longitudinal scheme [35] and our two-tone modulation readout. In the examples shown in Figs. 2 and 3 we evolve to time scales of order κ^{-1} and we set the loss $\kappa = J_r/2$. The choice of this ratio is important in the sense that a smaller coupling would give a lower magnitude steady state, and a smaller SNR, while a smaller loss κ would give a slower overall readout time. In the normal dispersive readout, the equivalent requirement for a non-negligible SNR on this same time scale is

$$\frac{E}{\kappa} \frac{J_r^2}{\Delta} > \kappa/2, \tag{19}$$

where $\Delta = \omega_c - \Delta h$, and E is the magnitude of an external resonant drive on the cavity. However, due to the perturbative nature of the dispersive interaction, there is a limit on the value of $E/\kappa < (\Delta/\sqrt{8}J_r)$ (sometimes termed the "critical photon number" [69–74]). This in turn limits the value of κ one can allow in the dispersive readout scheme at least to $J_r/\sqrt{2}$, and in practice much less (the critical photon number is an extreme upper limit, related to how dressed the eigenstates of the dispersive Hamiltonian become at larger photon numbers). On the other hand, the longitudinal schemes function with high fidelity up to the "bad cavity" limit of $\kappa = J_r/2$ (as illustrated in Figs. 2 and 3), a regime which potentially offers faster readout (a related point regarding single-shot readout with longitudinal coupling, even in the bad cavity limit, was made by Beaudoin *et al.* [56]). For example, for the same parameters we use in the figures, the dispersive readout fails completely.

A. Finite exchange tunneling

As discussed in the Introduction, it was proposed in Ref. [53] that one can tune $J_0 \to 0$ by applying a large *global* magnetic field. However, in general there may be technical issues limiting how small J_0 can be made. In addition, even with negligible J_0 there may be be a residual time-dependant exchange tunneling arising when we modulate the height of the gate voltage. For completeness, we discuss the influence of these two imperfections on our results in Figs. 2 and 3. Returning to the Hamiltonian for the dot system,

$$H_d = \frac{J_0}{2}\sigma_x + \frac{\Delta h}{2}\sigma_z, \tag{20}$$

we define $J_0 = \bar{J}_0 + \delta J_0(t)$, i.e., an exchange tunneling with both a static and modulated part.

If $\bar{J}_0 = 0$, and the residual modulation of the exchange term has the same functional dependance as the modulated coupling, $\delta J_0(t) = \delta J_0 \cos(\Delta ht)\cos(\omega_c t)$, then the influence of this modulation on the QND-ness is negligible if $\delta J_0 \ll \omega_c \pm 2\Delta h, \omega_c$. We illustrate this in Figs. 2 and 3, where the red dashed curves show that a modulation with a magnitude equal to the spin-photon coupling in those figures has almost no influence on the SNR and QND-ness for this parameter range. However, nonzero δJ_0 does reduce the QND-ness and SNR around (but not at) the optimal point $\Delta h = \omega_c/2$, where the above RWA condition breaks down (we do not explicitly show this in the figures). Precisely at the optimal point $\Delta h = \omega_c/2$, the QND-ness and SNR are restored because the Hamiltonian again becomes of the QND form.

Conversely, if $\bar{J}_0$ is small but finite, and the accidental modulation of the exchange term is $\delta J_0(t) = 0$, we require $\bar{J}_0 \ll \Delta h$ for the influence of the static exchange tunneling to be negligible, as one might expect. This error can be mitigated to some degree by changing the modulation of the coupling term so that it is on resonance with the new eigenenergy of the qubit, $\omega_q = \sqrt{\Delta h^2 + \bar{J}_0^2}$. In this basis, the full Hamiltonian becomes

$$H = \frac{\omega_q}{2}\bar{\sigma}_z + \omega_c a^\dagger a + J_r \cos(\omega_q t)\cos(\omega_c t)[\sin(\theta)\bar{\sigma}_x$$
$$+ \cos(\theta)\bar{\sigma}_z](a + a^\dagger), \tag{21}$$

where $\theta = \arctan(\Delta h/\bar{J}_0)$.

Given this new Hamiltonian, we have two options, which are distinguished as option A and option B in the figures. In option A, we still assume the qubit starts in an eigenstate of the original-basis Pauli operator σ_x, and it is in that basis, and in the interaction picture of the $\omega_q \bar{\sigma}_z$ free Hamiltonian, that we evaluate the QND-ness and SNR in the orange dashed curves in Figs. 2 and 3. For $\bar{J}_0 = J_r$ the presence of this static $\bar{J}_0$ does reduce the QND-ness and SNR for small Δh, but this rapidly increases and becomes comparable to the ideal case around $\Delta h = 0.1\omega_c$. The SNR does not recover for $\Delta h = 0$ in this case because of the residual modulation of the coupling at $\bar{J}_0$ in this limit.

Alternatively, for option B, we change the basis of our readout such that the qubit is prepared, and measured, in an eigenstate of $\bar{\sigma}_x$. This implies that the error term, for finite J_0, is the residual $\cos(\theta)\bar{\sigma}_z$ part of the above Hamiltonian. This choice has a better performance for intermediate Δ_h, but fails completely when $\Delta_h \to 0$. This is trivially seen to be because, at $\Delta_h = 0$, our choice of initial state is not an eigenstate of the remaining coupling Hamiltonian, $\bar{\sigma}_z$.

Note that, for the same parameters, but modulating at just Δh, and using just the Δh part of the free Hamiltonian to define the interaction picture, and the measurement basis, there is a much larger reduction in the QND-ness around $\Delta h = \bar{J}_0$. We do not explicitly show this case in the figures, as it essentially performs worse than the above two options. Also not shown is the influence of both finite $\bar{J}_0$ and $\delta J_0(t)$ on options A and B, as the influence of the static $\bar{J}_0$ is the dominant contribution for the parameters shown in the figures.

IV. AMPLIFIED TRANSVERSE COUPLING REGIME

The magnitudes of the spin-photon coupling strengths predicted in theory [8,53], and seen in experiments so far [20–22], are in the strong-coupling regime (in that it exceeds the qubit and cavity losses). However, they are still far from the ultra-strong-coupling regime [41–43,45–47], as they are orders of magnitude smaller than the qubit or cavity frequency themselves. In addition, in the system we describe in this paper, the singlet-triplet spin qubit is typically off-resonant with the cavity. If one wishes to realize effective resonant interactions, or even simulate [48–52] certain aspects of the ultra-strong-coupling regime, one can do so by modulating the qubit-cavity coupling, $J_r(t)$, to make the influence of the qubit on the cavity again akin to a resonant force. One can do this by now choosing

$$J_r(t) = J_r \cos(\omega_d t), \tag{22}$$

in which case the total Hamiltonian becomes

$$H = \frac{J_0}{2}\sigma_x + \frac{\Delta h}{2}\sigma_z + \omega_c a^\dagger a + J_r \cos(\omega_d t)\sigma_x(a + a^\dagger).$$

Applying a standard transformation $U = \exp(i\omega_d a^\dagger a t)$, this Hamiltonian becomes

$$\begin{aligned} H = {} & \frac{J_0}{2}\sigma_x + \frac{\Delta h}{2}\sigma_z + (\omega_c - \omega_d)a^\dagger a \\ & + J_r \cos(\omega_d t)\sigma_x(ae^{-i\omega_d t} + a^\dagger e^{i\omega_d t}). \end{aligned} \qquad (23)$$

Applying the RWA, assuming $\Delta h, J_r \ll \omega_d$, in the limit that J_0 is negligible, one obtains

$$H^R = \frac{\Delta h}{2}\sigma_z + (\omega_c - \omega_d)a^\dagger a + \frac{J_r}{2}\sigma_x(a + a^\dagger). \qquad (24)$$

For resonant interactions, one can choose $(\omega_c - \omega_d) = \Delta h$. As the effective cavity frequency is reduced, the influence of the qubit on the cavity is amplified. To realize certain aspects of the ultra-strong-coupling regime one can choose $(\omega_d - \omega_c) = 0$, thus, as in the longitudinal case, entering a frame where the cavity frequency vanishes. In principle, this would also allow one to study a nonequilibrium variant of the single-qubit Dicke phase transition [34], similar to the nonequilibrium Dicke phase transition model studied by Bastidas *et al.* [75].

V. CONCLUSIONS

In this paper we showed how a two-tone modulation of the coupling between a qubit, as exemplified with the singlet-triplet states in a double quantum dot, and a cavity allows one to switch between transverse and longitudinal coupling schemes. While being more "approximate" than a purely engineered longitudinal coupling, and thus not perfectly QND in some regimes, this approach allows one to switch between transverse and longitudinal coupling, as required. For the latter, we present a detailed perturbative analysis in the Appendix, to show the robustness of the scheme for realistic parameters. Finally, we argued that the longitudinal scheme can be used in the bad cavity (large κ) limit, in principle allowing for a faster readout. Of course, this approach can also be applied to traditional circuit-QED [35], and perhaps also to other approaches to spin-photon coupling [8,20,21].

APPENDIX

In this Appendix we present a perturbative analysis which explains the different features of Figs. 2 and 3 for the case where the exchange tunneling J_0 is zero. We will do this for a full range of Δh from zero to ω_c. Specifically, in Sec. 1 of this Appendix, we identify the regimes where the full dynamics can (or cannot) be well approximated by a QND time-independent Hamiltonian. In Sec. 2 of this Appendix, we present a higher-order approximation of such an effective dynamics. Finally, we present two figures, complementary to Figs. 2 and 3 presented in the main text for the QND and SNR, over the full range of Δh.

1. Perturbative analysis

Starting from the full Hamiltonian,

$$\begin{aligned} H = {} & \frac{\Delta h}{2}\sigma_z + \omega_c a^\dagger a \\ & + J_r \cos(\omega_c t)\cos(\Delta h t)\sigma_x(a + a^\dagger), \end{aligned} \qquad (A1)$$

with two-tone modulation of the coupling, we will perform a perturbative analysis of the different regimes lying in the range $0 \leqslant \Delta h \leqslant \omega_c$.

It is convenient to write the previous Hamiltonian in a frame $|\tilde{\Psi}\rangle = U|\Psi\rangle$, with $U = \exp\{i[\omega_c a^\dagger a + (\Delta h/2)\sigma_z]t\}$ as

$$\begin{aligned} H = {} & J_r \cos(\omega_c t)\cos(\Delta h t)(e^{i\Delta h t}\sigma_+ + e^{-i\Delta h t}\sigma_-) \\ & \times (e^{i\omega_c t}a^\dagger + e^{-i\omega_c t}a) \\ = {} & H_0 + \sum_{n_{\Delta h},n_C=-1,0,1} H_{n_{\Delta h}n_c} e^{2i(n_{\Delta h}\Delta h + n_c\omega_c)} \end{aligned} \qquad (A2)$$

where

$$\begin{aligned} H_0 &= \frac{J_r}{4}\sigma_x(a + a^\dagger), \\ H_{1,0} &= \frac{J_r}{4}(a + a^\dagger)\sigma_+, \\ H_{0,1} &= \frac{J_r}{4}\sigma_x a^\dagger, \\ H_{1,1} &= \frac{J_r}{4}\sigma_+ a^\dagger, \quad \text{and} \\ H_{-1,1} &= \frac{J_r}{4}\sigma_- a^\dagger \end{aligned} \qquad (A3)$$

with $H_{-n_{\Delta h},-n_c} = H_{n_{\Delta h},n_c}^\dagger$ and $H_{0,0} = 0$.

In the following we assume $J_r/\omega_c < 1$ and, for formal convenience, define

$$\tilde{J}_r = \frac{J_r}{8}. \qquad (A4)$$

In the following, we will (1) perform an initial RWA to write $H = H^{\text{RWA}} + O(\tilde{J}_r^2/\omega_c)$ and (2) perform an additional approximation, to put the rotating-wave Hamiltonian in a QND form, i.e.,

$$H \rightarrow H_{\text{eff}} \propto H_0. \qquad (A5)$$

This will be achieved by either (1) an additional RWA, to neglect terms which rotate at a frequency ω satisfying $\lambda_{\text{RWA}}(\omega) = \tilde{J}_r/\omega < 1$, or (2) an adiabatic approximation (A),

to neglect slowly rotating terms at frequency ω satisfying $\lambda_A(\omega) = \omega/\tilde{J}_r = 1/\lambda_{\mathrm{RWA}} < 1$.

The error of this approximation depends on the specific range of parameters considered. Specifically, we will analyze the regimes $0 < \Delta h < \omega_c/2$ and $\omega_c/2 < \Delta h < \omega_c$ separately.

a. Regime $0 < \Delta h < \omega_c/2$. When $0 < \Delta h < \omega_c/2$, the frequencies $\omega_c - \Delta h, \omega_c, \Delta h + \omega_c$ appearing in the Hamiltonian in Eq. (A2) are $O(\omega_c)$. Keeping the most relevant error, the RWA allows us to write

$$H = H_{\Delta h}^{\mathrm{RWA}} + O\left(\frac{\tilde{J}_r^2}{\omega_c}\right) \tag{A6}$$

where

$$H_{\Delta h}^{\mathrm{RWA}} = H_0 + 2\tilde{J}_r(a + a^\dagger)(e^{2i\Delta ht}\sigma_+ + e^{-2i\Delta ht}\sigma_-). \tag{A7}$$

To proceed further, we need to analyze the perturbative parameters λ_{RWA} and λ_A for the time-dependent part of the previous Hamiltonian.

(1) When $0 < \Delta h < \tilde{J}_r$, we have $\lambda_{\mathrm{RWA}}(\Delta h) = \tilde{J}_r/\Delta h > 1$ and $\lambda_A(\Delta h) = 1/\lambda_{\mathrm{RWA}}(\Delta h) < 1$, which is compatible with an adiabatic approximation. In fact, for times $t < \tau$ with $\tau = 1/\tilde{J}_r$ (consistent with the choices $T = 1/\kappa, 2/\kappa$ and $\kappa = J_r/2 = 4\tilde{J}_r$ used for the simulations), the condition $0 < \Delta h < \tilde{J}_r$ allows one to expand the exponentials in Eq. (A7) at first order in $(\Delta h\, t)$, to obtain

$$H_{\Delta h}^{\mathrm{RWA}} = 2H_0 + O(\Delta h) \tag{A8}$$

so that, in this regime, $H_{\mathrm{eff}} = 2H_0$. The quality of this approximation degrades as $\Delta h \to \tilde{J}_r$.

(2) When $\Delta h = \tilde{J}_r$, the frequency of the time-dependent term becomes equal to its energy scale and $\lambda_{\mathrm{RWA}}(\tilde{J}_r) = \lambda_A(\tilde{J}_r)$ and neither a further RWA nor the adiabatic approximation is allowed.

(3) When $\tilde{J}_r < \Delta h < \omega_c/2$, we have $\lambda_{\mathrm{RWA}}(\Delta h) = \tilde{J}_r/\Delta h < 1$ and $\lambda_A(\Delta h) = 1/\lambda_{\mathrm{RWA}}(\Delta h) > 1$, which allows us to perform an additional RWA, giving

$$H_{\Delta h}^{\mathrm{RWA}} = H_0 + O\left(\frac{\tilde{J}_r^2}{\Delta h}\right) \tag{A9}$$

so that, in this regime, $H_{\mathrm{eff}} = H_0$.

b. Regime $\omega_c/2 < \Delta h < \omega_c$. When $\omega_c/2 < \Delta h < \omega_c$, the frequencies $\Delta h, \omega_c, \Delta h + \omega_c$ appearing in the Hamiltonian in Eq. (A2) are $O(\omega_c)$. Keeping the most relevant error, the RWA

allows us to write

$$H = H_{\omega_c - \Delta h}^{\mathrm{RWA}} + O\left(\frac{\tilde{J}_r^2}{\omega_c}\right) \tag{A10}$$

where

$$H_{\omega_c - \Delta h}^{\mathrm{RWA}} = H_0 + 2\tilde{J}_r[e^{2i(\omega_c - \Delta h)t}\sigma_- a^\dagger$$
$$+ e^{-2i(\omega_c - \Delta h)t}\sigma_+ a]. \tag{A11}$$

Again, to proceed further, we need to analyze the perturbative parameters λ_{RWA} and λ_A.

(1) When $\omega_c/2 < \Delta h < \omega_c - \tilde{J}_r$, we have $\lambda_{\mathrm{RWA}}(\omega_c - \Delta h) = \tilde{J}_r/(\omega_c - \Delta h) < 1$ and $\lambda_A(\omega_c - \Delta h) = 1/\lambda_{\mathrm{RWA}}(\omega_c - \Delta h) > 1$, which again allows us to perform a further RWA to write

$$H_{\omega_c - \Delta h}^{\mathrm{RWA}} = H_0 + O\left(\frac{\tilde{J}_r^2}{(\omega_c - \Delta h)}\right) \tag{A12}$$

so that, in this regime $H_{\mathrm{eff}} = H_0$.

(2) When $\Delta h = \omega_c - \tilde{J}_r$ the frequency of the time-dependent term becomes equal to its energy scale and $\lambda_{\mathrm{RWA}}(\omega_c - \tilde{g}) = \lambda_A(\omega_c - \tilde{J}_r)$; once again neither a further RWA nor the adiabatic approximation is allowed.

(3) When $\omega_c - \tilde{J}_r < \Delta h < \omega_c$, we have $\lambda_{\mathrm{RWA}}(\omega_c - \Delta h) = \tilde{J}_r/(\omega_c - \Delta h) > 1$, and $\lambda_A(\omega_c - \Delta h) = 1/\lambda_{\mathrm{RWA}}(\omega_c - \Delta h) < 1$, which once again allows us to perform an adiabatic approximation. For times $t < \tau$ with $\tau = 1/\tilde{J}_r$ (again consistent with the choices $T = 1/\kappa, 2/\kappa$ and $\kappa = J_r/2 = 4\tilde{J}_r$ used in the simulations), the condition $\omega_c - \tilde{J}_r < \Delta h < \omega_c$ allows one to expand the exponentials in Eq. (A11) at first order in $(\omega_c - \Delta h)t$ to obtain

$$H_{\omega_c - \Delta h}^{\mathrm{RWA}} = H_0 + 2\tilde{J}_r(\sigma_- a^\dagger + \sigma_+ a) + O(\omega_c - \Delta h)$$
$$= H_0 + O(\omega_c - \Delta h) + O(\tilde{J}_r) \tag{A13}$$

so that, in this regime, $H_{\mathrm{eff}} = H_0$. The quality of this approximation degrades as $\Delta h \to \omega_c - \tilde{J}_r$.

The results of this analysis are collected in Table I. Most importantly, from Eq. (A9) and Eq. (A12) we see that the scaling of errors is minimized for $\Delta h = \omega_c/2$, justifying our suggestion, in the main text, of $\Delta h = \omega_c/2$ being the optimal working point.

2. High-frequency regime

Deep in the high-frequency regime, where the condition $\tilde{J}_r \ll \Delta h \ll \omega_c - \tilde{J}_r$ is satisfied, all time-dependent contribu-

TABLE I. In this table we summarize the analysis in the Appendix. For each parameter range, our goal is to identify the error in approximating the behavior as an effective QND Hamiltonian H_{eff}. These errors are minimized at the trivial extreme point $\Delta h = 0$, where we return to the intrinsically longitudinal case studied elsewhere. More interestingly, in the regime of interest of this paper ($\tilde{J}_r < \Delta h < \omega_c - \tilde{J}_r$), the scaling of the errors suggests the presence of another optimal point at $\Delta h = \omega_c/2$.

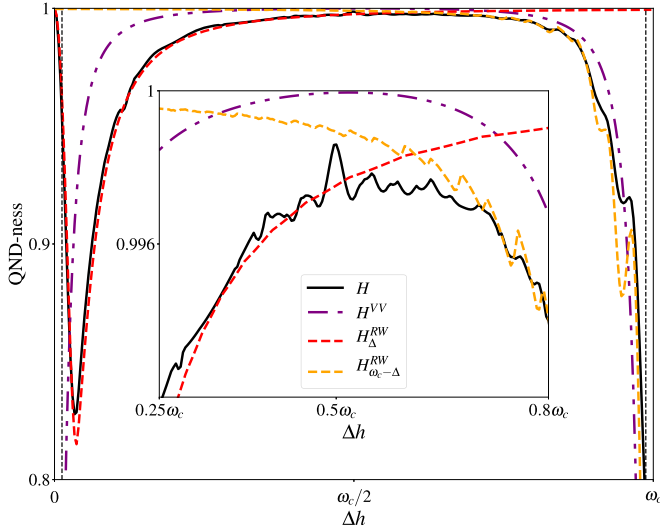| Range	RWA: $H = H^{\mathrm{RWA}} + O(\tilde{J}_r^2/\omega_c)$	Regime	H_{eff}	$H_{\mathrm{eff}} - H^{\mathrm{RWA}}$
$\Delta h = 0$	$H_0^{\mathrm{RWA}} = 2H_0$		$2H_0$	0
$0 < \Delta h < \tilde{J}_r$	$H_{\Delta h}^{\mathrm{RWA}} = H_0 + 2\tilde{J}_r(a + a^\dagger)(e^{2i\Delta ht}\sigma_+ + e^{-2i\Delta ht}\sigma_-)$	Adiabatic	$2H_0$	$O(\Delta h)$
$\tilde{J}_r < \Delta h < \frac{\omega_c}{2}$	$H_{\Delta h}^{\mathrm{RWA}} = H_0 + 2\tilde{J}_r(a + a^\dagger)(e^{2i\Delta ht}\sigma_+ + e^{-2i\Delta ht}\sigma_-)$	High-freq.	H_0	$O(\tilde{J}_r^2/\Delta h)$
$\frac{\omega_c}{2} < \Delta h < \omega_c - \tilde{J}_r$	$H_{\omega_c - \Delta h}^{\mathrm{RWA}} = H_0 + 2\tilde{J}_r[e^{2i(\omega_c - \Delta h)t}\sigma_- a^\dagger + e^{-2i(\omega_c - \Delta h)t}\sigma_+ a]$	High-freq.	H_0	$O(\tilde{J}_r^2/(\omega_c - \Delta h))$
$\omega_c - \tilde{J}_r < \Delta h < \omega_c$	$H_{\omega_c - \Delta h}^{\mathrm{RWA}} = H_0 + 2\tilde{J}_r[e^{2i(\omega_c - \Delta h)t}\sigma_- a^\dagger + e^{-2i(\omega_c - \Delta h)t}\sigma_+ a]$	Adiabatic	H_0	$O(\omega_c - \Delta h) + O(\tilde{J}_r)$
$\Delta h = \omega_c$	$H_{\omega_c}^{\mathrm{RWA}} = H_0 + 2\tilde{J}_r(\sigma_- a^\dagger + \sigma_+ a)$		H_0	$O(\tilde{J}_r)$

FIG. 4. As in Fig. 2, we plot the QND fidelity of the measurement process QND fidelity $\mathrm{Min}[\langle|+\rangle\langle+|\rangle]_\tau$ for an initial excited state $|+\rangle$ as a function of Δh. In this figure we use larger coupling magnitude, $J_r = 0.1\omega_c$, and loss $\kappa = J_r/2$, to accentuate the deviation from the ideal QND behavior. As before we choose the total integration time $\tau = 2/\kappa$. In black is the result for the full system Hamiltonian while the other lines correspond to the effective Hamiltonians listed in Table I in the Appendix. The black dashed vertical lines represent the points $\Delta h = \{\tilde{J}_r, \omega_c - \tilde{J}_r\}$, which set the boundary between the adiabatic and high-frequency regimes (which, for the reasons explained in the text, we expect to be valid in the long measurement time limit, i.e., when $\kappa\tau \to \infty$). It is clear that operating at the point $\Delta h = \omega_c/2$ is optimal, as also suggested by our perturbative analysis, apart from the point corresponding to $\Delta h = 0$, where the Hamiltonian is intrinsically longitudinal (corresponding to the proposal in Ref. [35]). The inset zooms on the parameter regime $0.2\omega_c < \Delta h < 0.8\omega_c$.

tions to the original Hamiltonian H satisfy $\lambda_{\mathrm{RWA}} \ll 1$ and a more rigorous analysis can be performed. By using Van Vleck perturbation theory in Floquet space [76–78] an alternative effective Hamiltonian [see Eq. (14) in the main text] can be written as

$$
\begin{aligned}
H^{\mathrm{VV}} &= DHD^{-1} \\
&= H_0 - \frac{1}{2}\sum_{n_{\Delta h} n_C = -1,0,1} \frac{[H_{-n_{\Delta h},-n_C}, H_{n_{\Delta h}, n_C}]}{2n_{\Delta h}\Delta h + 2n_C\omega_c} \\
&\quad + O\left(\frac{\tilde{J}_r^3}{\Delta h^2}\right) + O\left(\frac{\tilde{J}_r^3}{\omega_c^2}\right) + O\left(\frac{\tilde{J}_r^3}{(\omega_c - \Delta h)^2}\right) \\
&\quad + O\left(\frac{\tilde{J}_r^3}{(\omega_c + \Delta h)^2}\right) \\
&= H_0 + (2\tilde{J}_r)^2\left[\frac{(a + a^\dagger)^2}{2\Delta h} - \frac{\Delta h}{\omega_c^2 - \Delta h^2}\left(a^\dagger a + \frac{1}{2}\right)\right]\sigma_z
\end{aligned}
$$
(A14)

in a frame defined as $D = \exp[-iS(t)]$, with

$$
S(t) = \sum_{n_{\Delta h}, n_C} \frac{iH_{n_{\Delta h}, n_c}}{2n_{\Delta h}\Delta h + 2n_c\omega_c} F_{n_{\Delta h}} F_{n_c},
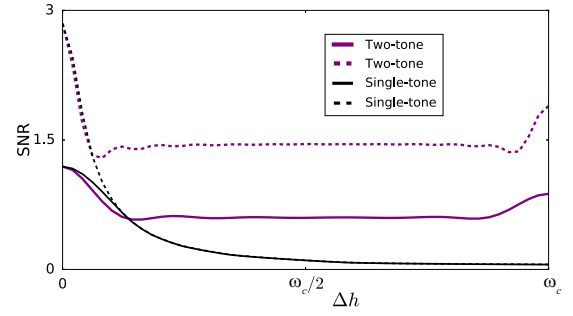$$
(A15)

FIG. 5. For completeness, as in Fig. 3 we show the SNR as a function of Δh, with other parameters as in Fig. 4. As expected, the SNR is large at $\Delta h = \omega_c/2$, and maximal for $\Delta h \to 0$. The solid lines are for $\tau = 1/\kappa$, while the dashed lines are for $\tau = 2/\kappa$, illustrating how one acquires more signal for longer measurement periods. The purple curves are for our two-tone modulation scheme, while the black lines show the behavior when one modulates the coupling at just the cavity frequency.

where $F_{n_{\Delta h}} = \exp(2in_{\Delta h}\Delta h t)$, $F_{n_c} = \exp(2in_c\omega_c t)$. The appearance of σ_z at this order suggests it is the first non-QND term that arises (recalling that our scheme is performing measurements in the σ_x basis, such that evolution due to σ_z terms will cause deviations from the desired QND behavior).

We note that the Floquet resonances defined by the intuitive condition

$$
n_1\Delta h + n_2\omega_c + n_3(\omega_c + \Delta h) + n_4(\omega_c - \Delta h) \ll J_r/4
$$
(A16)

with $|n_i - n_j| = \pm 1, 0$ for $i, j = 1, 2, 3, 4$ are due to a skewed description of the system as a more appropriate description can be found in terms of slow envelopes of the remaining high-frequency pulses. As a consequence, the usual high-frequency approximations in Floquet space can be supported by adiabatic considerations [79–81] leading to Eq. (A14).

For completeness, it is also worth taking into consideration the tilting of the frame described in Eq. (A15) in which the Van Vleck Hamiltonian is valid. For example, at $t = 0$, the change of frame is already nontrivial (although highly suppressed in the high-frequency regime) and reads

$$
S(0) = \sum_{n_{\Delta h}, n_c} \frac{iH_{n_{\Delta h}, n_c}}{2n_{\Delta h}\Delta h + 2n_c\omega_c}.
$$
(A17)

By undoing this change of frame with the operator $D_0 = \exp(-iS_0)$ we get

$$
\begin{aligned}
H_0^{VV} &= D_0^{-1}DHD^{-1}D_0, \\
&= D_0^{-1}H^{VV}D_0, \\
&= H^{VV} - i[H_0, S(0)] + O\left(\frac{g^3}{\Delta h^2}\right), \\
&= H^{VV} + \sum_{n_{\Delta h}, n_c} \frac{[H_0, H_{n_{\Delta h}, n_c}]}{2n_{\Delta h}\Delta h + 2n_c\omega_c},
\end{aligned}
$$
(A18)

and, finally,

$$
H_0^{VV} = H_0 + (2\tilde{J}_r)^2\left\{\frac{(a + a^\dagger)^2}{2\Delta h} - \frac{\Delta h}{\omega_c^2 - \Delta h^2}\left(a^\dagger a + \frac{1}{2}\right)\right.
$$

$$- \frac{(a + a^\dagger)}{\Delta h} + \frac{\Delta h}{\omega_c^2 - \Delta h^2} [1 + (a + a^\dagger)^2] \Big\} \sigma_z. \quad (A19)$$

To compare the different levels of approximations studied in this Appendix, we finish by presenting, in Fig. 4, the QND fidelity over the full range of Δh, complementing Fig. 2 in the main text. In Fig. 5 we also present the SNR for the same range of Δh, complementing Fig. 3 in the main text.

[1] L. Childress, A. S. Sørensen, and M. D. Lukin, Mesoscopic cavity quantum electrodynamics with quantum dots, Phys. Rev. A **69**, 042302 (2004).

[2] C. Bergenfeldt and P. Samuelsson, Microwave quantum optics and electron transport through a metallic dot strongly coupled to a transmission line cavity, Phys. Rev. B **85**, 045446 (2012).

[3] N. Lambert, C. Flindt, and F. Nori, Photon-mediated electron transport in hybrid circuit-QED, Europhys. Lett. **103**, 17005 (2013).

[4] L. D. Contreras-Pulido, C. Emary, T. Brandes, and R. Aguado, Non-equilibrium correlations and entanglement in a semiconductor hybrid circuit-QED system, New J. Phys. **15**, 95008 (2013).

[5] C. Bergenfeldt and P. Samuelsson, Nonlocal transport properties of nanoscale conductor-microwave cavity systems, Phys. Rev. B **87**, 195427 (2013).

[6] M. R. Delbecq, V. Schmitt, F. D. Parmentier, N. Roch, J. J. Viennot, G. Fève, B. Huard, C. Mora, A. Cottet, and T. Kontos, Coupling a Quantum Dot, Fermionic Leads, and a Microwave Cavity on a Chip, Phys. Rev. Lett. **107**, 256804 (2011).

[7] T. Frey, P. J. Leek, M. Beck, A. Blais, T. Ihn, K. Ensslin, and A. Wallraff, Dipole Coupling of a Double Quantum Dot to a Microwave Resonator, Phys. Rev. Lett. **108**, 046807 (2012).

[8] X. Hu, Y. X. Liu, and F. Nori, Strong coupling of a spin qubit to a superconducting stripline cavity, Phys. Rev. B **86**, 035314 (2012).

[9] T. Frey, P. J. Leek, M. Beck, J. Faist, A. Wallraff, K. Ensslin, T. Ihn, and M. Büttiker, Quantum dot admittance probed at microwave frequencies with an on-chip resonator, Phys. Rev. B **86**, 115303 (2012).

[10] K. D. Petersson, L. W. McFaul, M. D. Schroer, M. Jung, J. M. Taylor, A. A. Houck, and J. R. Petta, Circuit quantum electrodynamics with a spin qubit, Nature (London) **490**, 380 (2012).

[11] M. R. Delbecq, L. E. Bruhat, J. J. Viennot, S. Datta, A. Cottet, and T. Kontos, Photon-mediated interaction between distant quantum dot circuits. Nat. Commun. **4**, 1400 (2013).

[12] H. Toida, T. Nakajima, and S. Komiyama, Vacuum Rabi Splitting in a Semiconductor Circuit QED System, Phys. Rev. Lett. **110**, 066802 (2013).

[13] A. Wallraff, A. Stockklauser, T. Ihn, J. R. Petta, and A. Blais, Comment on "Vacuum Rabi Splitting in a Semiconductor Circuit QED System," Phys. Rev. Lett. **111**, 249701 (2013).

[14] J. J. Viennot, M. R. Delbecq, M. C. Dartiailh, A. Cottet, and T. Kontos, Out-of-equilibrium charge dynamics in a hybrid circuit quantum electrodynamics architecture, Phys. Rev. B **89**, 165404 (2014).

[15] Y.-Y. Liu, J. Stehlik, C. Eichler, M. J. Gullans, J. M. Taylor, and J. R. Petta, Semiconductor double quantum dot micromaser, Science **347**, 285 (2015).

[16] A. Stockklauser, V. F. Maisi, J. Basset, K. Cujia, C. Reichl, W. Wegscheider, T. Ihn, A. Wallraff, and K. Ensslin, Microwave Emission from Hybridized States in a Semiconductor Charge Qubit, Phys. Rev. Lett. **115**, 046802 (2015).

[17] G. W. Deng, D. Wei, S. X. Li, J. R. Johansson, W. C. Kong, H. O. Li, G. Cao, M. Xiao, G. C. Guo, F. Nori, H. W. Jiang, and G. P. Guo, Coupling two distant double quantum dots with a microwave resonator, Nano Lett. **15**, 6620 (2015).

[18] J. J. Viennot, M. C. Dartiailh, A. Cottet, and T. Kontos, Coherent coupling of a single spin to microwave cavity photons. Science **349**, 408 (2015).

[19] F. Beaudoin, D. Lachance-Quirion, W. A. Coish, and M. Pioro-Ladrière, Coupling a single electron spin to a microwave resonator: Controlling transverse and longitudinal couplings, Nanotechnology **27**, 464003 (2016).

[20] X. Mi, M. Benito, S. Putz, D. M. Zajac, J. M. Taylor, G. Burkard, and J. R. Petta, A coherent spin-photon interface in silicon, Nature (2017), doi:10.1038/nature25769

[21] N. Samkharadze, G. Zheng, N. Kalhor, D. Brousse, A. Sammak, U. C. Mendes, A. Blais, G. Scappucci, and L. M. K. Vandersypen, Strong spin-photon coupling in silicon, Science **359**, 1123 (2018).

[22] A. J. Landig, J. V. Koski, P. Scarlino, U. C. Mendes, A. Blais, C. Reichl, W. Wegscheider, A. Wallraff, K. Ensslin, and T. Ihn, Coherent spin-qubit photon coupling, arXiv:1711.01932 (2017).

[23] L. E Bruhat, T. Cubaynes, J. J. Viennot, M. C. Dartiailh, M. M. Desjardins, A. Cottet, and T. Kontos, Strong coupling between an electron in a quantum dot circuit and a photon in a cavity, arXiv:1612.05214.

[24] X. Mi, J. V. Cady, D. M. Zajac, P. W. Deelman, and J. R. Petta, Strong coupling of a single electron in silicon to a microwave photon, Science **355**, 156 (2017).

[25] A. Stockklauser, P. Scarlino, J. V. Koski, S. Gasparinetti, C. K. Andersen, C. Reichl, W. Wegscheider, T. Ihn, K. Ensslin, and A. Wallraff, Strong Coupling Cavity QED with Gate-Defined Double Quantum Dots Enabled by a High Impedance Resonator, Phys. Rev. X **7**, 011030 (2017).

[26] X. Mi, J. V. Cady, D. M. Zajac, J. Stehlik, L. F. Edge, and J. R. Petta, Circuit quantum electrodynamics architecture for gate-defined quantum dots in silicon, Appl. Phys. Lett. **110**, 043502 (2017).

[27] Y. Mu and C. M. Savage, One-atom lasers, Phys. Rev. A **46**, 5944 (1992).

[28] J. McKeever, A. Boca, A. D. Boozer, J. R. Buck, and H. J. Kimble, Experimental realization of a one-atom laser in the regime of strong coupling, Nature (London) **425**, 268 (2003).

[29] O. Astafiev, K. Inomata, A. O. Niskanen, T. Yamamoto, Yu. A. Pashkin, Y. Nakamura, and J. S. Tsai, Single artificial-atom lasing, Nature (London) **449**, 588 (2007).

[30] S. Ashhab, J. R. Johansson, A. M. Zagoskin, and F. Nori, Single-artificial-atom lasing using a voltage-biased superconducting charge qubit, New J. Phys. **11**, 23030 (2009).

[31] M. Cirio, S. De Liberato, N. Lambert, and F. Nori, Ground State Electroluminescence, Phys. Rev. Lett. **116**, 113601 (2016).

[32] N. Lambert, F. Nori, and C. Flindt, Bistable Photon Emission from a Solid-State Single-Atom Laser, Phys. Rev. Lett. **115**, 216803 (2015).

[33] C. Bergenfeldt, P. Samuelsson, B. Sothmann, C. Flindt, and M. Buttiker, Hybrid Microwave-Cavity Heat Engine, Phys. Rev. Lett. **112**, 076803 (2014).

[34] S. Ashhab, Superradiance transition in a system with a single qubit and a single oscillator, Phys. Rev. A **87**, 013826 (2013).

[35] N. Didier, J. Bourassa, and A. Blais, Fast Quantum Nondemolition Readout by Parametric Modulation of Longitudinal Qubit-Oscillator Interaction, Phys. Rev. Lett. **115**, 203601 (2015).

[36] B. Royer, A. L. Grimsmo, N. Didier, and A. Blais, Fast and high-fidelity entangling gate through parametrically modulated longitudinal coupling, Quantum **1**, 11 (2016).

[37] Y. J. Zhao, Y. L. Liu, Y. X. Liu, and F. Nori, Generating nonclassical photon states via longitudinal couplings between superconducting qubits and microwave fields, Phys. Rev. A **91**, 053820 (2015).

[38] X. Wang, A. Miranowicz, H.-R. Li, and F. Nori, Multiple-output microwave single-photon source using superconducting circuits with longitudinal and transverse couplings, Phys. Rev. A **94**, 053858 (2016).

[39] X. Wang, A. Miranowicz, H. R. Li, and F. Nori, Hybrid quantum device with a carbon nanotube and a flux qubit for dissipative quantum engineering, Phys. Rev. B **95**, 205415 (2017).

[40] X. Wang, A. Miranowicz, H.-R. Li, and F. Nori, Observing pure effects of counter-rotating terms without ultrastrong coupling: A single photon can simultaneously excite two qubits, Phys. Rev. A **96**, 063820 (2017)..

[41] C. Ciuti, G. Bastard, and I. Carusotto, Quantum vacuum properties of the intersubband cavity polariton field, Phys. Rev. B **72**, 115303 (2005).

[42] J. Casanova, G. Romero, I. Lizuain, J. J. García-Ripoll, and E. Solano, Deep Strong Coupling Regime of the Jaynes-Cummings Model, Phys. Rev. Lett. **105**, 263603 (2010).

[43] S. Ashhab and F. Nori, Qubit-oscillator systems in the ultrastrong-coupling regime and their potential for preparing nonclassical states, Phys. Rev. A **81**, 042311 (2010).

[44] X. Gu, A. F. Kockum, A. Miranowicz, Y.-X. Liu, and F. Nori, Microwave photonics with superconducting quantum circuits, Phys. Rep. **718–719**, 1 (2017).

[45] R. Stassi, V. Macrì, A. F. Kockum, O. Di Stefano, A. Miranowicz, S. Savasta, and F. Nori, Quantum nonlinear optics without photons, Phys. Rev. A **96**, 023818 (2017).

[46] R. Stassi and F. Nori, Long-lasting quantum memories: Extending the coherence time of superconducting artificial atoms in the ultrastrong-coupling regime, Phys. Rev. A **97**, 033823 (2018).

[47] A. F. Kockum, A. Miranowicz, V. Macrì, S. Savasta, and F. Nori, Deterministic quantum nonlinear optics with single atoms and virtual photons, Phys. Rev. A **95**, 063849 (2017).

[48] D. Ballester, G. Romero, J. J. García-Ripoll, F. Deppe, and E. Solano, Quantum Simulation of the Ultrastrong-Coupling Dynamics in Circuit Quantum Electrodynamics, Phys. Rev. X **2**, 021007 (2012).

[49] A. L. Grimsmo and S. Parkins, Cavity-QED simulation of qubit-oscillator dynamics in the ultrastrong-coupling regime, Phys. Rev. A **87**, 033814 (2013).

[50] J. Braumüller, M. Marthaler, A. Schneider, A. Stehli, H. Rotzinger, M. Weides, and A. V. Ustinov, Analog quantum simulation of the Rabi model in the ultra-strong coupling regime, Nat. Commun. **8**, 779 (2017).

[51] N. K. Langford, R. Sagastizabal, M. Kounalakis, C. Dickel, A. Bruno, F. Luthi, D. J. Thoen, A. Endo, and L. DiCarlo, Experimentally simulating the dynamics of quantum light and matter at deep-strong coupling, Nat. Commun. **8**, 1715 (2017).

[52] D. Lv, S. An, Z. Liu, J.-N. Zhang, J. S. Pedernales, L. Lamata, E. Solano, and K. Kim, Quantum simulation of the quantum Rabi model in a trapped ion, arXiv:1711.00582 (2017).

[53] P. Q. Jin, M. Marthaler, A. Shnirman, and G. Schön, Strong Coupling of Spin Qubits to a Transmission Line Resonator, Phys. Rev. Lett. **108**, 190506 (2012).

[54] A. M. Satanin, M. V. Denisenko, A. I. Gelman, and F. Nori, Amplitude and phase effects in Josephson qubits driven by a biharmonic electromagnetic field, Phys. Rev. B **90**, 104516 (2014).

[55] S. Hacohen-Gourgy, L. S. Martin, E. Flurin, V. V. Ramasesh, K. B. Whaley, and I. Siddiqi, Quantum dynamics of simultaneously measured non-commuting observables, Nature (London) **538**, 491 (2016).

[56] F. Beaudoin, A. Blais, and W. A. Coish, Hamiltonian engineering for robust quantum state transfer and qubit readout in cavity QED, New J. Phys. **19**, 023041 (2017).

[57] G. Burkard, D. Loss, and D. P. DiVincenzo, Coupled quantum dots as quantum gates, Phys. Rev. B **59**, 2070 (1999).

[58] G. Burkard, G. Seelig, and D. Loss, Spin interactions and switching in vertically tunnel-coupled quantum dots, Phys. Rev. B **62**, 2581 (2000).

[59] J. Pedersen, C. Flindt, N. A. Mortensen, and A. P. Jauho, Failure of standard approximations of the exchange coupling in nanostructures, Phys. Rev. B **76**, 125323 (2007).

[60] J. G. Pedersen, C. Flindt, A. P. Jauho, and N. A. Mortensen, Influence of confining potentials on the exchange coupling in double quantum dots, Phys. Rev. B **81**, 193406 (2010).

[61] J. Medford, J. Beil, J. M. Taylor, E. I. Rashba, H. Lu, A. C. Gossard, and C. M. Marcus, Quantum-Dot-Based Resonant Exchange Qubit, Phys. Rev. Lett. **111**, 050501 (2013).

[62] M. Pioro-Ladrière, T. Obata, Y. Tokura, Y.-S. Shin, T. Kubo, K. Yoshida, T. Taniyama, and S. Tarucha, Electrically driven single-electron spin resonance in a slanting Zeeman field, Nat. Phys. **4**, 776 (2008).

[63] N. Lambert, I. Mahboob, M. Pioro-Ladriere, Y. Tokura, S. Tarucha, and H. Yamaguchi, Electron-Spin Manipulation and Resonator Readout in a Double-Quantum-Dot Nanoelectromechanical System, Phys. Rev. Lett. **100**, 136802 (2008).

[64] S. Ashhab, J. R. Johansson, A. M. Zagoskin, and F. Nori, Two-level systems driven by large-amplitude fields, Phys. Rev. A **75**, 063414 (2007).

[65] J. R. Johansson, P. D. Nation, and F. Nori, QuTiP: An open-source Python framework for the dynamics of open quantum systems, Comput. Phys. Commun. **183**, 1760 (2012).

[66] J. R. Johansson, P. D. Nation, and F. Nori, QuTiP 2: A Python framework for the dynamics of open quantum systems, Comput. Phys. Commun. **184**, 1234 (2013).

[67] H. M. Wiseman and G. J. Milburn, *Quantum Measurement and Control* (Cambridge University, Cambridge, England, 2009).

[68] B. Fan, A. F. Kockum, J. Combes, G. Johansson, I. C. Hoi, C. M. Wilson, P. Delsing, G. J. Milburn, and T. M. Stace, Breakdown of the Cross-Kerr Scheme for Photon Counting, Phys. Rev. Lett. **110**, 053601 (2013).

[69] J. Q. You and F. Nori, Quantum information processing with superconducting qubits in a microwave field, Phys. Rev. B **68**, 064509 (2003).

[70] A. Blais, R. S. Huang, A. Wallraff, S. M. Girvin, and R. J. Schoelkopf, Cavity quantum electrodynamics for superconducting electrical circuits: An architecture for quantum computation, Phys. Rev. A **69**, 062320 (2004).

[71] J. Q. You and F. Nori, Superconducting circuits and quantum information, Phys. Today **58**, 42 (2005).

[72] M. Boissonneault, J. M. Gambetta, and A. Blais, Nonlinear dispersive regime of cavity QED: The dressed dephasing model, Phys. Rev. A **77**, 060305 (2008).

[73] M. Boissonneault, J. M. Gambetta, and A. Blais, Dispersive regime of circuit QED: Photon-dependent qubit dephasing and relaxation rates, Phys. Rev. A **79**, 013819 (2009).

[74] J. Q. You and F. Nori, Atomic physics and quantum optics using superconducting circuits, Nature (London) **474**, 589 (2011).

[75] V. M. Bastidas, C. Emary, B. Regler, and T. Brandes, Nonequilibrium Quantum Phase Transitions in the Dicke Model, Phys. Rev. Lett. **108**, 043003 (2012).

[76] M. Leskes, P. K. Madhu, and S. Vega, Floquet theory in solid-state nuclear magnetic resonance, Prog. Nucl. Magn. Reson. Spectrosc. **57**, 345 (2010).

[77] A. Eckardt, Atomic quantum gases in periodically driven optical lattices, Rev. Mod. Phys. **89**, 11004 (2017).

[78] S. Kohler, J. Lehmann, and P. Hänggi, Driven quantum transport on the nanoscale, Phys. Rep. **406**, 379 (2004).

[79] V. Novičenko, E. Anisimovas, and G. Juzeliūnas, Floquet analysis of a quantum system with modulated periodic driving, Phys. Rev. A **95**, 023615 (2017).

[80] C. De Grandi and A. Polkovnikov, Adiabatic perturbation theory: From Landau-Zener problem to quenching through a quantum critical point, in *Quantum Quenching, Annealing and Computation*, edited by A. K. Chandra, A. Das, and B. K. Chakrabarti (Springer, Berlin, 2010), pp. 75–114.

[81] P. Weinberg, M. Bukov, L. D'Alessio, A. Polkovnikov, S. Vajna, and M. Kolodrubetz, Adiabatic perturbation theory and geometry of periodically-driven systems, Phys. Rep. **688**, 1 (2017).